Extensive Biotransformation Profiling of AZD8205, an Anti-B7-H4 Antibody-Drug Conjugate, Elucidates Pathways Underlying its Stability *In Vivo*

Yue Huang[1]*, Hui Yin Tan[1], Jiaqi Yuan[1], Ruipeng Mu[1], Junyan Yang[1], Kathryn Ball[2], Balakumar Vijayakrishnan[3], Luke Masterson[3], Krista Kinneer[4], Nadia Luheshi[5], Meina Liang[1], Anton I. Rosenbaum[1]*

[1]Integrated Bioanalysis, Clinical Pharmacology and Safety Sciences, R&D, AstraZeneca, South San Francisco, CA 94080, USA
[2]Clinical Pharmacology and Quantitative Pharmacology, Clinical Pharmacology and Safety Sciences, R&D, AstraZeneca, Cambridge CB21 6GH United Kingdom
[3]TTD, Oncology R&D, AstraZeneca, London E1 2AX, United Kingdom
[4]Translational Medicine, Oncology R&D, AstraZeneca, Gaithersburg, MD 20878, USA
[5] Oncology R&D, AstraZeneca, Cambridge CB2 8PA, United Kingdom

*Corresponding Authors
Yue Huang - 121 Oyster Point Blvd, South San Francisco, CA 94080, USA; Tel: +1-650-481-6801; E-mail: yhuang@revmed.com
Anton I. Rosenbaum - 121 Oyster Point Blvd, South San Francisco, CA 94080, USA; Tel: +1-650-379-3099; E-mail: anton.rosenbaum@astrazeneca.com

Abstract

What happens to macromolecules *in vivo*? What drives structure-activity relationship and *in vivo* stability for antibody-drug conjugates (ADCs)? These interrelated questions are increasingly relevant due to re-emerging importance of ADCs as an impactful therapeutic modality and the gaps that exist in our understanding of ADC structural determinants that underlie ADC *in vivo* stability. Complex macromolecules, such as ADCs, may undergo changes *in vivo* due to their intricate structure as biotransformations may occur on the linker, the payload and/or at the modified conjugation site. Dissection of ADC metabolism presents a substantial analytical challenge due to the difficulty in identification or quantification of minor changes on a large macromolecule. We employed immunocapture-LCMS methods to evaluate *in vivo* changes in DAR profile in four different lead ADCs. This resulted in selection of AZD8205, a B7-H4-directed cysteine-conjugated ADC bearing a topoisomerase I inhibitor payload, with durable DAR. The results showed that vast majority of the biotransformation species identified contained at least one payload. This comprehensive characterization revealed that critical structural determinant contributing to the design of AZD8205 was the PEG section of the linker, resulting in competition between linker deconjugation and maleimide hydrolysis reactions resulting in a durable high DAR *in vivo*. To our knowledge, this study is the most extensive characterization of ADC *in vivo* biotransformation to date, which also sheds light on determinants of ADC stability *in vivo* and informs the selection of optimal linker. These results highlight the relevance of studying macromolecule biotransformation in elucidating the ADC structure-*in vivo* stability relationship.

Introduction

Structural characterization of macromolecules *in vitro* has advanced significantly over the past decades. A plethora of techniques have been employed to characterize the structure of a protein macromolecule primary sequence as well as secondary and tertiary structure at atomic and sub-atomic resolution. Advanced techniques are applied to characterize molecular dynamics of molecules[1] and recent advances have focused on characterization of macromolecular complexes and non-covalent interactions[2]. In case of small molecules, the structural characterization *in vitro* has been extended to the *in vivo* realm under the auspices of biotransformation analyses, and biotransformation of small molecule xenobiotics is well understood and characterized. However, characterization of changes to protein macromolecule structure *in vitro* as well *in vivo*, i. e. biotransformation, is an emerging area of scientific inquiry[3, 4]. The main biotransformation pathway for traditional protein therapeutics usually involves straightforward proteolysis[5]. Therefore, recent work in macromolecule biotransformation has focused primarily on characterization of complex biotherapeutics such as antibody-drug conjugates (ADCs)[6-8].

ADCs combine the high specificity of monoclonal antibodies (mAbs) and potent cytotoxic drugs connected by a cleavable or non-cleavable linker for targeted drug payload delivery[9]. Presently, 15 ADCs have obtained approval from Food and Drug Administration (FDA) or European Medicines Agency (EMA)[10]. ADCs are designed to stay intact while in circulation and release their drug payload upon target-mediated internalization into tumor cells, maximizing therapeutic index (TI). The linker design plays a major role in modulating the timing and location of drug release[11]. However, biotransformation of ADCs, such as payload deconjugation or modification to the antibody, drug or linker can impact their *in vivo* stability[5, 12]. Hence, in-depth characterization of biotransformations of ADCs would aid in their chemical optimization influencing *in vivo* stability.

Bioanalytical strategies for the quantification and characterization of novel bioconjugate therapeutics have been thoroughly discussed over the past several years[4, 13]. Typical approaches for ADC quantification in support of pharmacokinetic assessments entail monitoring only surrogate analytes (peptides/payloads) via a targeted bottom-up approach. Therefore, information of the biotransformation is typically lost without a priori knowledge. High resolution accurate mass spectrometry (HRMS) based intact analysis of ADCs coupled with chromatographic separation is a powerful tool for the identification of novel biotransformation species. Recent advances in the field of HRMS in addition to more efficient ionization of macromolecules enable the progress of analyzing intact biotherapeutics such as mAbs and ADCs[14, 15].

AZD8205 is a B7-H4-targeted ADC utilizing a novel topoisomerase I linker-payload[16] (**Figure** 1) being studied in the clinic for the treatment of biliary tract, breast, ovarian or endometrial cancers (NCT05123482)[17, 18]. As part of the structure-activity relationship (SAR) optimization of AZD8205 we examined 4 different linkers to enable the conjugation of the topoisomerase I payload (TOP1i AZ14170132)[17]. The payload was covalently conjugated to native interchain cysteines of an anti-B7-H4 antibody via a Val-Ala (VA) or Gly-Gly-Phe-Gly (GGFG) peptide linker with or without a PEG8 spacer **(Figure** 1), resulting in four distinct anti-B7-H4 ADCs, each with an approximate drug-to-antibody ratio (DAR) of 8. To characterize AZD8205 pharmacokinetics and biotransformation using both *in vitro* incubation and *in vivo* plasma samples in mice dosed with AZD8205, we employed intact and bottom-up

approaches. For bottom-up approaches, both collision-induced dissociation (CID) and electron-activated dissociation (EAD) methods using different fragmentation mechanism were applied to offer complementary insights. Herein, we describe the most comprehensive characterization of pharmacokinetics and biotransformation of an ADC from both *in vitro* and *in vivo* samples to date, employing orthogonal approaches providing complementary information. The findings confirmed durable structural and conjugation stability of AZD8205 among the 4 linker designs evaluated.

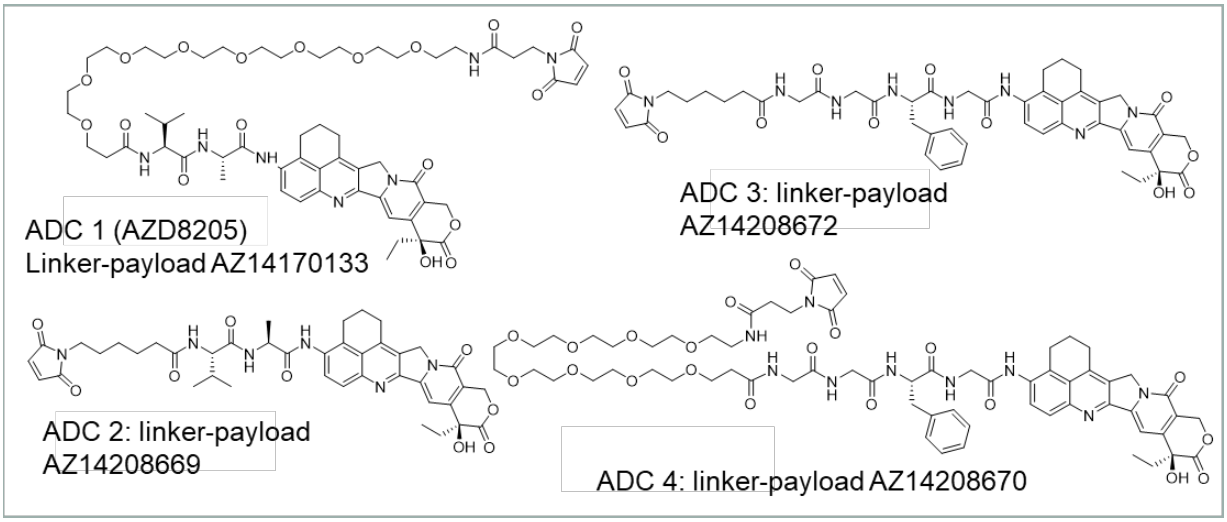

Figure 1. Schematic representation of the linker-payload structures evaluated.

Materials and Methods

Materials and Reagents

All ADCs, payload and stable isotope labeled payload, anti-idiotype antibody and anti-payload antibody used were provided by AstraZeneca (Gaithersburg, MD). Anti hu-Fc capture antibody was purchased from Bethyl. Peptide internal standards were custom synthesized by Vivitide. The pooled plasma was purchased from BioIVT. The SMART IA magnetic beads, tris(hydroxymethyl)aminomethane (Tris) buffer, Phosphate-buffered saline (PBS), Zeba 7K MWCO spin column, formic acid (FA), trifluoroacetic acid (TFA), and sulfo-NHS biotin were all purchased from Thermo Scientific. Bovine serum albumin and papain were purchased from Sigma-Aldrich. The chromatographic columns (BEH C18 and BioResolve) were purchased from Waters. All other reagents were purchased from VWR.

Pharmacokinetic Study in Tg32 Mice

All animal experiments were conducted in a facility accredited by the Association for Assessment and Accreditation of Laboratory Animal Care under the guidelines of AstraZeneca's Institutional Animal Care and Use Committee and appropriate animal research approvals. A single dose of the four ADC drug candidates (**Figure** 1) was administered intravenously to male SCID FcRn-/- hFcRn (32) Tg ("Tg32") mice (Strain #:018441, Jackson Laboratories, Bar Harbor, ME) at 5 mg/kg (n=9 per group). Plasma (K2EDTA as anti-coagulant) samples were collected post-dose 0.5, 6, 24, 48, 144, 288 h (n=3 for each timepoint).

LC-MRM Method for Quantification of Total Antibody, Intact Antibody and ADC Concentration

Calibration curve standards and Quality Control samples were prepared in blank pooled CD-1 mouse plasma using reference standard AZD8205. Calibration range was 0.100-15.0 µg/mL. AZD8205 was then enriched by immunoaffinity capture using SMART IA streptavidin beads conjugated to biotinylated anti human-Fc with approximately 2h incubation at ambient temperature. After separating the beads from supernatant and extensive washing of the beads, SMART IA digestion buffer with stable isotope-labeled internal standard was added to beads for tryptic digestion at 70 °C for 2h. After trypsin digestion, one fraction of the supernatant was used for total antibody and intact antibody assay. The other fraction was further digested using papain to release AZ14170132 for ADC assay. The characteristic peptides were quantified as surrogate analytes for the total antibody and intact antibody concentrations and the released AZ14170132 served as the surrogate analyte for the ADC concentration. The ADC concentration included all species of biotransformed molecules with payload in a DAR sensitive manner, regardless of linker biotransformations. All three assays were analyzed on the SCIEX Triple Quadrupole 6500+ mass spectrometer coupled with a Shimadzu liquid chromatography system. Chromatographic separation was performed using Waters ACQUITY UPLC BEH C18 Column (PN186002350). Mobile phases were A: 0.1 % formic acid in water and B: 0.1 % formic acid in acetonitrile. Data were acquired and analyzed with Analyst (v1.7) and MultiQuant (v3.0.3863) software, respectively.

For each ADC, the naïve pooled plasma concentration-time data obtained after a single 5 mg/kg IV administration in Tg32 mice using a sparse sampling design were used to estimate mean PK parameters for ADC, total antibody and intact antibody using noncompartmental analysis in Phoenix WinNonlin version 6.4 (Certara, NJ, USA). Concentrations that were below the limit of quantification of the assay were excluded from the PK parameter analysis. The area under the plasma concentration–time curve (AUClast) was calculated by using the linear-up log-down trapezoidal method, and the maximum serum concentration (Cmax), plasma clearance (CL), volume of distribution at steady state (Vss), and terminal elimination half-life (T1/2, z) were also estimated.

Intact LC-HRMS Profiling of Biotransformation Species

An intact LC-HRMS assay was developed to characterize ADC biotransformation species from *in vitro* and *in vivo* samples. This method allows a more specific identification of various biotransformation species as well as unbiased quantification. For each sample, the ADC concentration was first measured with the LBA-LC-MRM assay. Plasma concentrations were then adjusted to achieve 8.3 µg/mL ADC with a 120 µL aliquot enabling capture of 1 µg ADC. For certain samples with low concentrations where 1 µg of ADC was not achievable, the maximum volume of original plasma available was used (**Table** S1) in capture step. The plasma sample and SMART IA magnetic beads conjugated with biotinylated anti-human Fc (a-HuFc) or anti-payload antibody were incubated for approximately 30 min at ambient temperature to capture the ADC and its biotransformed species. After the removal of the supernatant following the capture step, the beads were then washed twice with PBS and then twice with water (250 µL each wash step). Finally, the ADC and biotransformed species were eluted off the beads by incubating the beads for 5 min with 45 µL 1% FA in water with cytochrome C. The samples were not deglycosylated or reduced to preserve the maximal information for identification of biotransformation species. The eluted samples were injected onto Shimadzu Nexera LC. The separation was performed on a Waters BioResolve

RP mAb polyphenyl column (PN186009017) with 1% FA, 0.01% TFA in water/ACN as mobile phases (example chromatogram in **Figure** 2A). A shallow gradient was applied in the reversed phase separation to resolve the various species and the major parent molecule. After LC, the separated species were then ionized and acquired in full scan mode with either SCIEX 6600 Triple TOF or 7600 Zeno TOF system.

Deconvolution, identification and quantification of Intact LC-HRMS data

The mass spectra were deconvoluted using a research version PeakView (version number: 1.2.2.0) with a sliding window method. This approach converts every 3 spectra with m/z-time domain to deconvoluted spectra in mass-time domain. This preserves chromatographic features such as retention time. The automated method treated all data in a consistent manner, eliminating the analyst bias in peak selection. This deconvolution method also eliminated the potential impact from neighboring main peak with high signal intensity on the smaller biotransformed peaks with lesser signal intensity. The mass-time information was then used to manually identify the biotransformed species structures. To quantify the relative abundance of the various biotransformed species, the mass-time chromatograms were analyzed with MultiQuant software using automatic peak integration (MQ4) at the theoretical mass with +/- 50 ppm as the extraction range. Pre-spiked cytochrome C was used to monitor run performance. Extracted peak area of each species was normalized with injected ADC mass for comparison between timepoints. For relative quantification of biotransformation species (% species) at each timepoint, the percentage was calculated by dividing the sum peak area of a class of species that shared a common feature (e.g. all heavy chain species with G0F) by the sum peak area of all biotransformation species in that class, including parent species (e.g. all heavy chain species).

Structural Elucidation of Biotransformation Species with Bottom-Up LC-HRMS

In vitro incubation of AZD8205 (0.1 mg/mL) in pooled human or CD1 mouse plasma at 37 °C were performed for 0, 6, 24, 72, and 168 h. The samples were then processed with a protocol similar to total antibody LC-MRM assay as described above. The samples were analyzed on the SCIEX 7600 ZenoTOF mass spectrometer coupled with a Shimadzu liquid chromatography system. Waters ACQUITY UPLC BEH C18 Column (PN186002350) was used for chromatography separation using mobile phases (A: 0.1 % FA in water; B: 0.1 % FA in acetonitrile). Data was acquired in positive IDA mode as well as TOF full scan MS2 mode in both CID and EAD for specific m/z of interest. Further data analysis including structural elucidation was performed with SCIEX OS software.

Results

Characterization of Pharmacokinetics with LBA-LC-MRM

The most common approach to understand biotransformation is to use a surrogate analyte method and measure fragments from the region of interest to indirectly confirm the structural integrity of the macromolecule[4, 19]. This was performed with LC-MRM methods for all ADCs in this study. The LBA-LC-MRM method was used to generate absolute quantitative results for the total Ab, intact Ab and ADC assay (**Figure** S2, **Table** S2). The data generated using the three methods resulted in overlapping

concentration-time profiles for all four ADCs, suggesting that no significant de-conjugation was observed, and the protein scaffold remained stable. The differences in concentration-time profiles between the four ADCs with various linkers were not significant when characterized with LBA-LC-MRM assays, considering the 20% accuracy and precision acceptance criteria for the assays.

Determination of *in vivo* Biotransformation Pathway Informs AZD8205 Lead Selection

To understand the impact different cleavable linkers would have on *in vivo* DAR stability we further examined ADC biotransformation pathways using LBA-LC-HRMS approach. As shown in **Figure** 2A, the light chain and the heavy chain are well separated, with the biotransformed species of the light chain and heavy chain eluting in the area close to the parent light chain and the parent heavy chain. Second, to maximize the identification of the various biotransformed products and to facilitate quantification of these species in an unbiased manner, an automated deconvolution was performed with PeakView (research version), where each spectrum was deconvoluted separately and the m/z-time raw data are converted to a mass-time data. Third, manual identification of the major biotransformed species was performed based on the theoretical intact mass difference between the parent peak and the biotransformed species (**Figure** 2B). Then, extracted peak area from the chromatograph was used for quantification, Lastly, the chemical structures of these proposed biotransformed species were further confirmed with LC-MS/MS with CID and EAD using *in vitro* incubation samples that possessed the same biotransformation species (Figure S3-S6).

This approach unveiled various macromolecular biotransformed species from light chain (LC), heavy chain (HC) or half antibody, identified over the 12-day period post-dose of each ADC in Tg32 mice (**Figure** 2, **Table** 1). This structural information for AZD8205 was confirmed using bottom-up LC-MS/MS with two different fragmentation mechanisms: collision-induced dissociation (CID) and electron-activated dissociation (EAD). To perform relative quantification of complex biotransformation species, the various analytes were clustered based on the relevant characteristics to provide simplified metrics for profiling the *in vivo* mixture of ADC and its biotransformed species. There are two assumptions for relative characterization of this data set: 1) capture efficiency and ionization efficiency are reasonably comparable among species used for quantification; 2) the data processing is performed uniformly for all species regardless of the signal intensity of the biotransformation species.

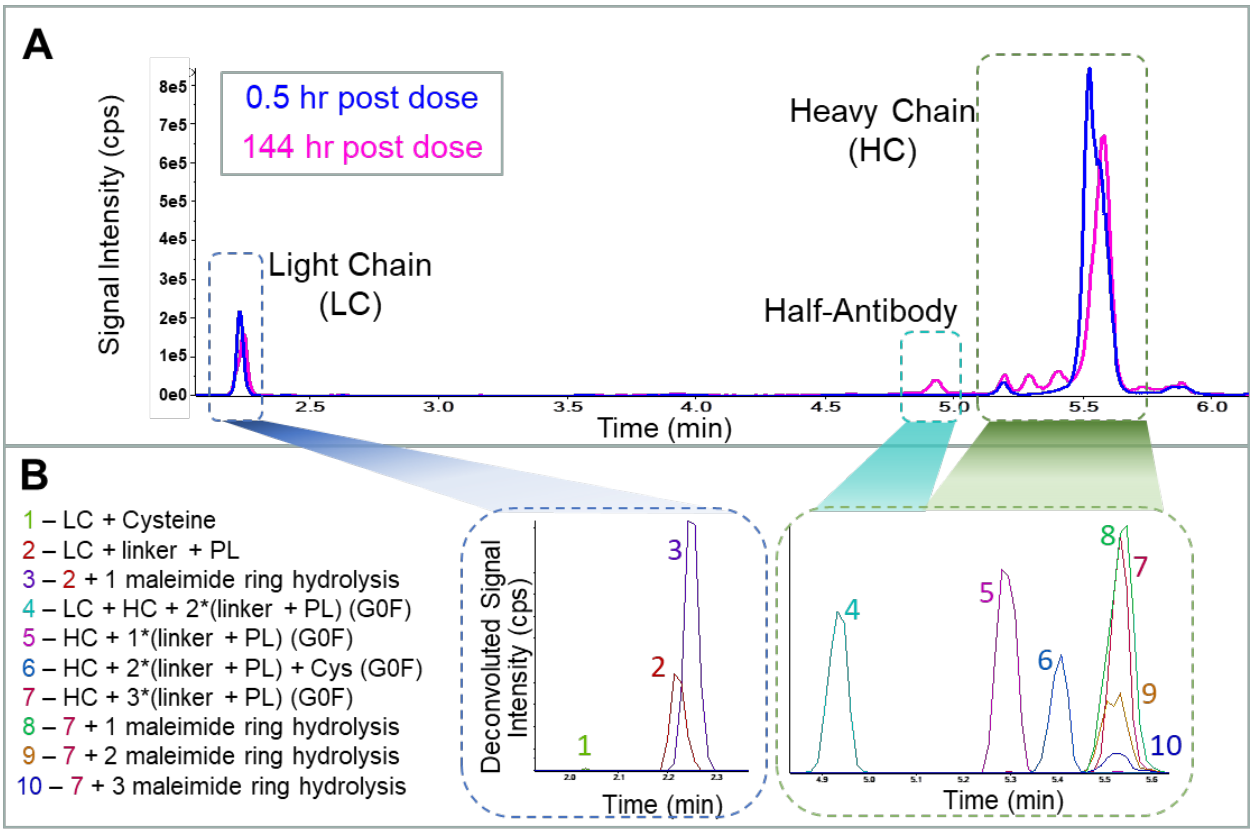

Figure 2. A. Representative total ion chromatogram for the ADCs, 0.5 hr and 144 hr post dose in human FcRn mice. B. Extracted ion chromatogram for selected major biotransformation species from deconvoluted data (mass-time) of peaks identified in A. LC: light chain, HC: heavy chain, PL: payload

Table 1: List of biotransformation species identified (PL: payload)

Index	Monitoring Species	Antibody Backbone	Payload	Glycosylation	Water	Other Modification	*Quantification
1	LC + 1(linker+ PL)	LC	1				✓
2	LC + 1(hydrolyzed linker+ PL)	LC	1		1		✓
3	LC	LC	0				✓
4	LC + Cys	LC	0			Cys	✓
5	HC + G0F	HC	0	G0F			✓
6	HC + G1F	HC	0	G1F			✓
7	HC + 1(linker+ PL) + G0F	HC	1	G0F			✓
8	HC + 1(linker+ PL) + G1F	HC	1	G1F			✓
9	HC + 1(hydrolyzed linker + PL) + G0F	HC	1	G0F	1		✓
10	HC + 1(hydrolyzed linker + PL) + G1F	HC	1	G1F	1		✓
11	HC + 2(linker+ PL) + G0F	HC	2	G0F			✓
12	HC + 2(linker+ PL) + G1F	HC	2	G1F			✓
13	HC + 1(linker+ PL) +1(hydrolyzed linker+ PL) + G0F	HC	2	G0F	1		✓
14	HC + 1(linker+ PL) +1(hydrolyzed linker+ PL) + G1F	HC	2	G1F	1		✓
15	HC + 2(hydrolyzed linker + PL) + G0F	HC	2	G0F	2		✓
16	HC + 2(hydrolyzed linker + PL) + G1F	HC	2	G1F	2		✓
17	HC + 2(linker + PL) + G0F + GSH	HC	2	G0F		GSH	
18	HC + 2(linker + PL) + G1F + GSH	HC	2	G1F		GSH	
19	HC + 2(linker + PL) + G0F + Cys	HC	2	G0F		Cys	✓
20	HC + 2(linker + PL) + G1F + Cys	HC	2	G1F		Cys	✓
21	HC + 1(linker+ PL) +1(hydrolyzed linker+ PL) + G0F + Cys	HC	2	G0F	1	Cys	✓
22	HC + 1(linker+ PL) +1(hydrolyzed linker+ PL) + G1F + Cys	HC	2	G1F	1	Cys	✓
23	HC + 2(hydrolyzed linker + PL) + G0F + Cys	HC	2	G0F	2	Cys	✓
24	HC + 2(hydrolyzed linker + PL) + G1F + Cys	HC	2	G1F	2	Cys	✓
25	HC + 3(linker+ PL) + G0F	HC	3	G0F			✓
26	HC + 3(linker+ PL) + G1F	HC	3	G1F			✓
27	HC + 2(linker+ PL) +1(hydrolyzed linker+ PL) + G0F	HC	3	G0F	1		✓
28	HC + 2(linker+ PL) +1(hydrolyzed linker+ PL) + G1F	HC	3	G1F	1		✓
29	HC + 1(linker+ PL) +2(hydrolyzed linker+ PL) + G0F	HC	3	G0F	2		✓
30	HC + 1(linker+ PL) +2(hydrolyzed linker+ PL) + G1F	HC	3	G1F	2		✓
31	HC + 3(hydrolyzed linker+ PL) + G0F	HC	3	G0F	3		✓
32	HC + 3(hydrolyzed linker+ PL) + G1F	HC	3	G1F	3		✓
33	LC + HC + 2(linker+ PL) + G0F	LC + HC	2	G0F			✓
34	LC + HC + 2(linker+ PL) + G1F	LC + HC	2	G1F			✓
35	LC + HC + 1(linker+ PL) +1(hydrolyzed linker+ PL) + G0F	LC + HC	2	G0F	1		✓
36	LC + HC + 1(linker+ PL) +1(hydrolyzed linker+ PL) + G1F	LC + HC	2	G1F	1		✓
37	LC + HC + 2(hydrolyzed linker+ PL) + G0F	LC + HC	2	G0F	2		✓
38	LC + HC + 2(hydrolyzed linker+ PL) + G1F	LC + HC	2	G1F	2		✓
39	Albumin		0				
40	Albumin + Cys		0			Cys	
41	Albumin + 1(linker+ PL)		1				✓
42	Albumin + 1(hydrolyzed linker+ PL)		1		1		✓

*Quantification marked out the species used to generate the relative quantification results in **Figure**s 3, 4, S7B and S8.

Biotransformation Step 1: Hydrolysis or Deconjugation from the Conjugation Site

Maleimide-conjugated payloads go through two competing biotransformation reactions: hydrolysis or deconjugation[6]. It was previously demonstrated that some linkers can partially deconjugate, resulting in a protein-partially cleaved payload structure[7]. Aside from the maleimide ring hydrolysis, protein scaffold instability has also been reported[19] when the parent molecule has disrupted disulfide bonds. For ADC1 (PEG8-VA linker) and ADC4 (PEG8-GGFG linker), species with hydrolyzed maleimide ring were the major biotransformation products on both the heavy chain and the light chain (**Figure** 3B). The retention time of these species did not alter significantly compared to the parent molecule. At 48 h post dose, the hydrolyzed forms replaced the original species and became the most abundant form of light chain for ADC1 and ADC4 (**Figure** 3B). For the heavy chain species, the hydrolysis happened gradually: generating partially hydrolyzed species first, then shifting to fully hydrolyzed species. The kinetics of the hydrolysis is dependent on the chemistry of the linker: both ADC 1 and ADC 4 contain linkers with PEG groups, resulting in faster hydrolysis rate for the maleimide ring compared to ADC 2 and ADC 3 (**Figure** 3, S7). The hydrolyzed species were also confirmed with LBA-LC-HRMS bottom-up identification, through both accurate mass MS1 as well as MS2 spectra (**Figure** S3 **Table** S4). The LC deconjugates less compared to the HC for all ADCs. In contrast to ADC1 and ADC4, for ADC 2 and ADC 3, the deconjugation on HC was observed as the major form especially for timepoints after 48 h (**Figure** 3A). Deconjugation results in lower DAR species. These species usually elute earlier compared to the parent molecule. For heavy chain species, the parent heavy chain (with 3 payloads, HC-3PL) eluted around 5.6 min, with the biotransformed species eluting around 5.4 min (HC-2PL) and 5.3 min (HC-1PL), respectively (**Figure** 2B). Note that the degree of deconjugation on LC for all ADCs are consistently low (<0.4 %) compared to HC (**Figure** 3A).

Deconjugation can result from two possible reactions: 1) deconjugation at the conjugation site, exposing the free thiol; and 2) deconjugation from step-wise linker cleavage, generating a series of HC or LC species with partial linker. In evaluating ADC 1-4, only species consistent with reaction 1 deconjugation were observed. Therefore, the deconjugation process and hydrolysis process for ADC 1-4 are two competing reactions. There is a clear structure-stability relationship and *in vivo* biotransformation reaction preference observed between the ADCs with or without PEG-containing linker. This provides mechanistic basis for improved *in vivo* DAR stability for ADC1 (AZD8205) and ADC4 versus ADC2 and ADC3.

Relative quantification from biotransformed species

The DAR of the ADC post-dose is the critical parameter to assess ADC deconjugation over time. The DAR can be calculated by comparing the total Ab and ADC data from the absolute LC-MRM quantification (**Figure** S8A), or with the identified LC and HC species from relative intact LC-HRMS (**Figures** 2, 3, S8B). It is notable that both methods showed that ADCs with PEG-containing linker had a slower deconjugation rate over the time. The LC-HRMS assay was able to characterize the structural differences in various species and kinetics of associated reactions.

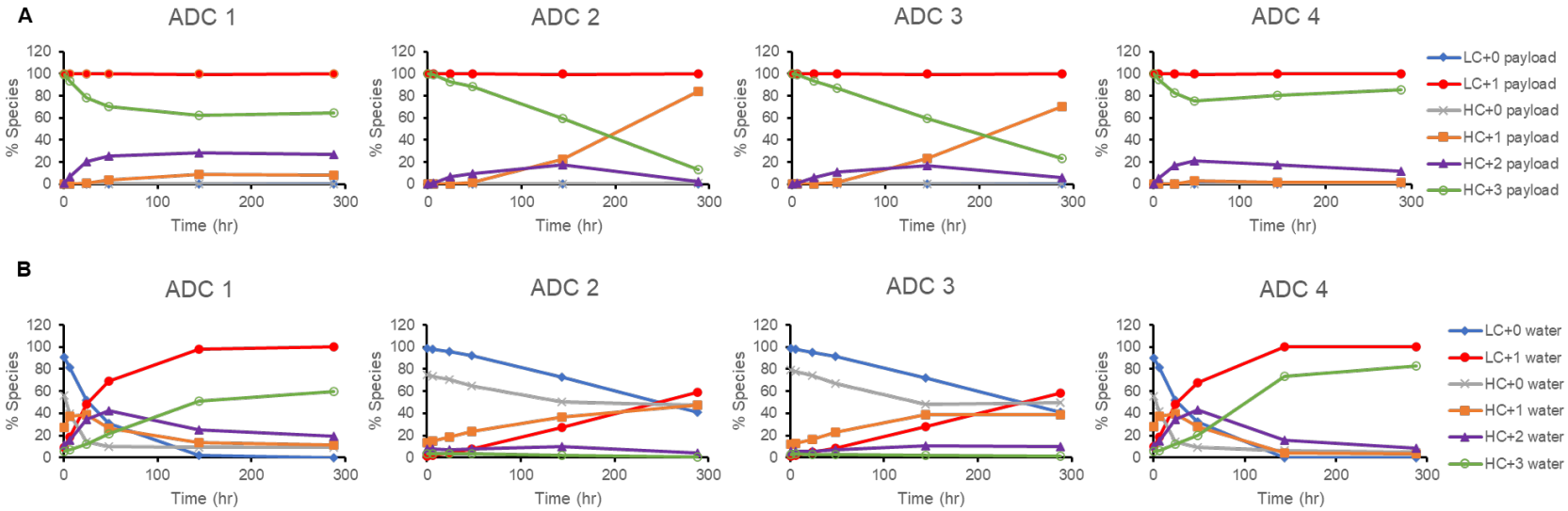

Figure 3. Changes in relative abundance of major biotransformation species for four ADC in mouse preclinical studies as function of time post-dose. A. Light and heavy chain species with varied numbers of conjugated payload(s). B. Maleimide hydrolysis species. LC: light chain, HC: heavy chain

Biotransformation Step 2: Reactions after Deconjugation

For the heavy chain and light chain with free thiol exposed, the observed biotransformation species were secondary reaction products including further formed cysteine and GSH adducts, and species with newly reformed disulfide bond between spatially close free thiols (**Figure** 4). This observation is supported with observed intact mass, and further confirmed with the MS2 fragmentation for selected parent ions from bottom-up LC-HRMS data (**Figures** S4-S6). The quantification of these secondary, minor, biotransformation species is displayed in **Figure** 4. Furthermore, the deconjugated small molecule linker-payload has been observed to covalently conjugate to circulating albumin (**Table** 1, index 41). The albumin-linker-payload can then next undergo maleimide ring hydrolysis (**Table** 1, index 42).

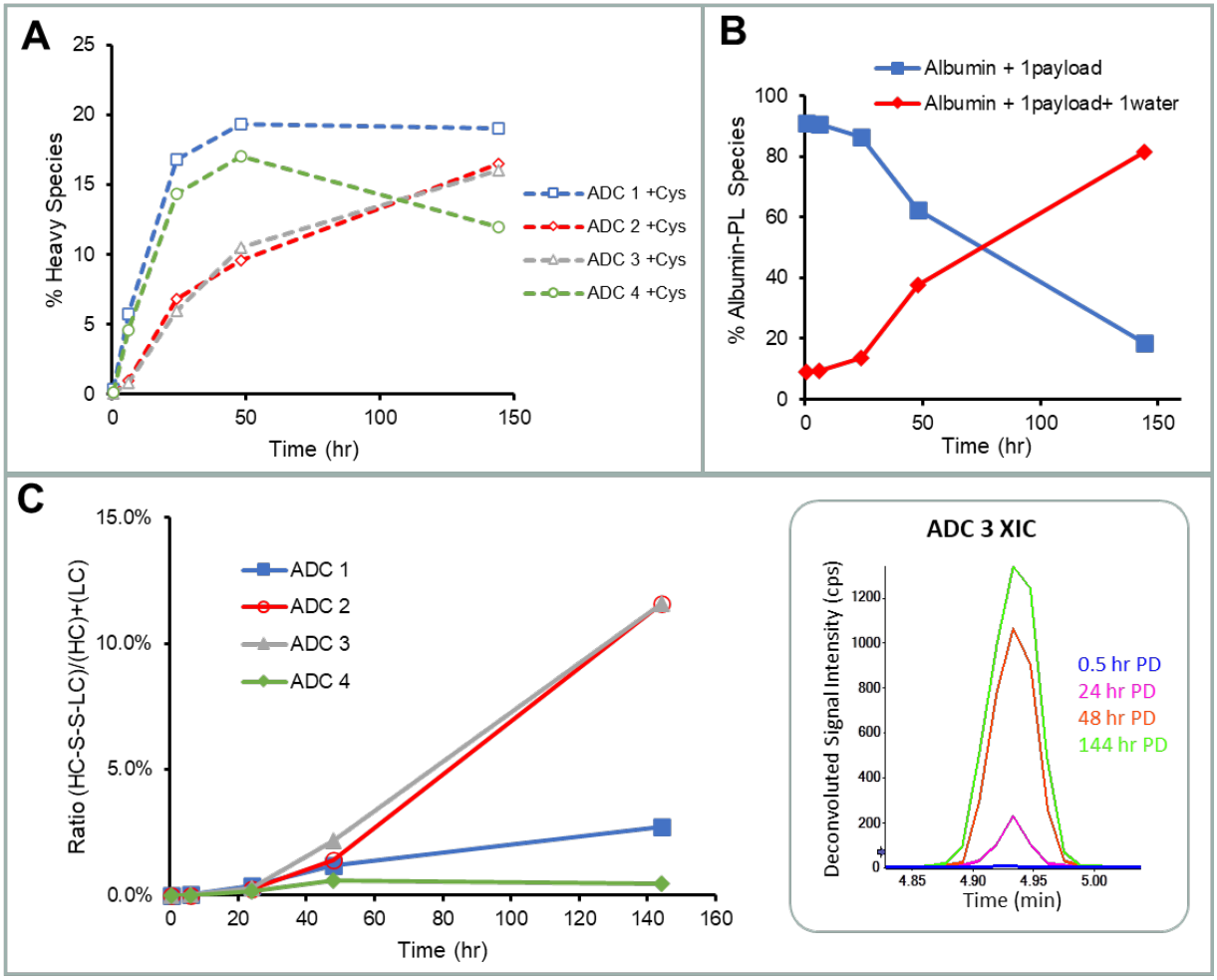

Figure 4. Secondary minor biotransformation reactions after linker-payload deconjugation. A) Cysteinylation change over time. B) Quantification of the maleimide hydrolysis of albumin-linker payload C) formation of the HC-LC inter chain disulfide bond increases with time, the inset figure showed the extracted ion chromatograph for ADC 3 at various timepoints. PD=post dose.

It is notable that the HC biotransformation species showed a distinct pattern when comparing the loss of one linker-payload and the loss of two linker-payloads. After deconjugation of a single linker-payload, we observed a cluster of peaks with several mass changes (**Figure** S9C, **Table** 1, index 11-24),

which are the multiple species formed after the exposed free thiol subsequently reacted with other redox-active molecules in plasma. The observed intact mass matched with the proposed adducts and the structure was further confirmed with CID MS2 spectra (**Figure** S4).On the contrary, after deconjugation of two linker-payloads, the major observed biotransformed species (**Table** 1, index 7-10) have a mass change of the loss of two linker-payloads (e.g. -2296 Da for AZD8205). No additional secondary adducts were observed. The potential reason of the distinct pattern after two payload loss is the reformation of the intra-chain disulfide bond. In the case of the HC-1PL species containing two free exposed thiols and if these thiols are spatially close, reformation of the intra chain disulfide bond becomes the major step 2 reaction. The heavy chain intra-chain disulfide bond was confirmed with bottom-up LC-HRMS with fragmentation (**Figure** S5).

Alternatively, the re-formation of disulfide bonds can happen between the light chain and the heavy chain, following payload deconjugation on both chains. This can be confirmed with the increasing amount of a 76 kD biotransformation species observed in the retention time (4.9 min) (**Figure** 4C, **Figure** S9A). The observed mass matched with the expected mass of light chain and heavy chain conjugated complex, with two linker-payloads remaining on the heavy chain and potential maleimide ring hydrolysis. This critical inter-chain disulfide bond between light chain-heavy chain was confirmed with bottom-up LC-HRMS with fragmentation (**Figure** S6). For ADCs that deconjugated to greater extent (ADC2 and ADC3), the potential of reformation of the interchain disulfide bond *in vivo* may have contributed to stabilization of the protein scaffold (**Figure** 3A, 4C, **Table** S2). Interchain disulfide bond reformation was observed for all 4 ADCs, although higher for ADC 2 and 3 (**Figure** 4C). This is likely due to the larger degree of deconjugation, catalyzing the re-formation of the disulfide bonds.After deconjugation, the deconjugated linker-payload can re-conjugate to various thiol-containing endogenous proteins[12]. Capture with anti-payload antibody enables detection and characterization of additional proteins that would contain the re-conjugated linker-payload, such as albumin. Interestingly, albumin conjugated linker-payload continued to hydrolyze over time (**Figure** 4B). These data are consistent with the hypothesis that the linker hydrolysis needs sufficient time for the reaction to proceed and the slower elimination half-life of albumin conjugated linker-payload enables this reaction to be observed on non-antibody containing macromolecular species. Further relative quantification analyses were also performed on the data set. The analysis suggested that glycoforms on the heavy chain do not seem to have a significant impact on the biotransformation at the conjugation site (**Figure** S10). Cysteinylation is the major secondary reaction for the exposed free thiol after deconjugation and also gradually increased over time (**Figure** 4A).

Maleimide-Conjugated Topoisomerase I inhibitor ADCs Biotransformation Pathways

Consolidating the information comprised of the observed biotransformation species proposed structures, their concentration-time profiles and common chemical reactions that can be expected under such circumstances, we propose the biotransformation pathways for ADC1-4 depicted in **Figure** 5. After dosing, the ADC can undergo two competing reactions: 1) hydrolysis on the maleimide linker, further stabilizing the conjugated payload and 2) deconjugation of the linker-payload, exposing the free thiol. For AZD8205, the vast majority of ADC went through reaction 1 as the main biotransformation pathway ensuring its *in vivo* stability. Upon deconjugation, further minor biotransformation products were

identified. This represents a very small, albeit analytically interesting fraction of the circulating ADC pool.

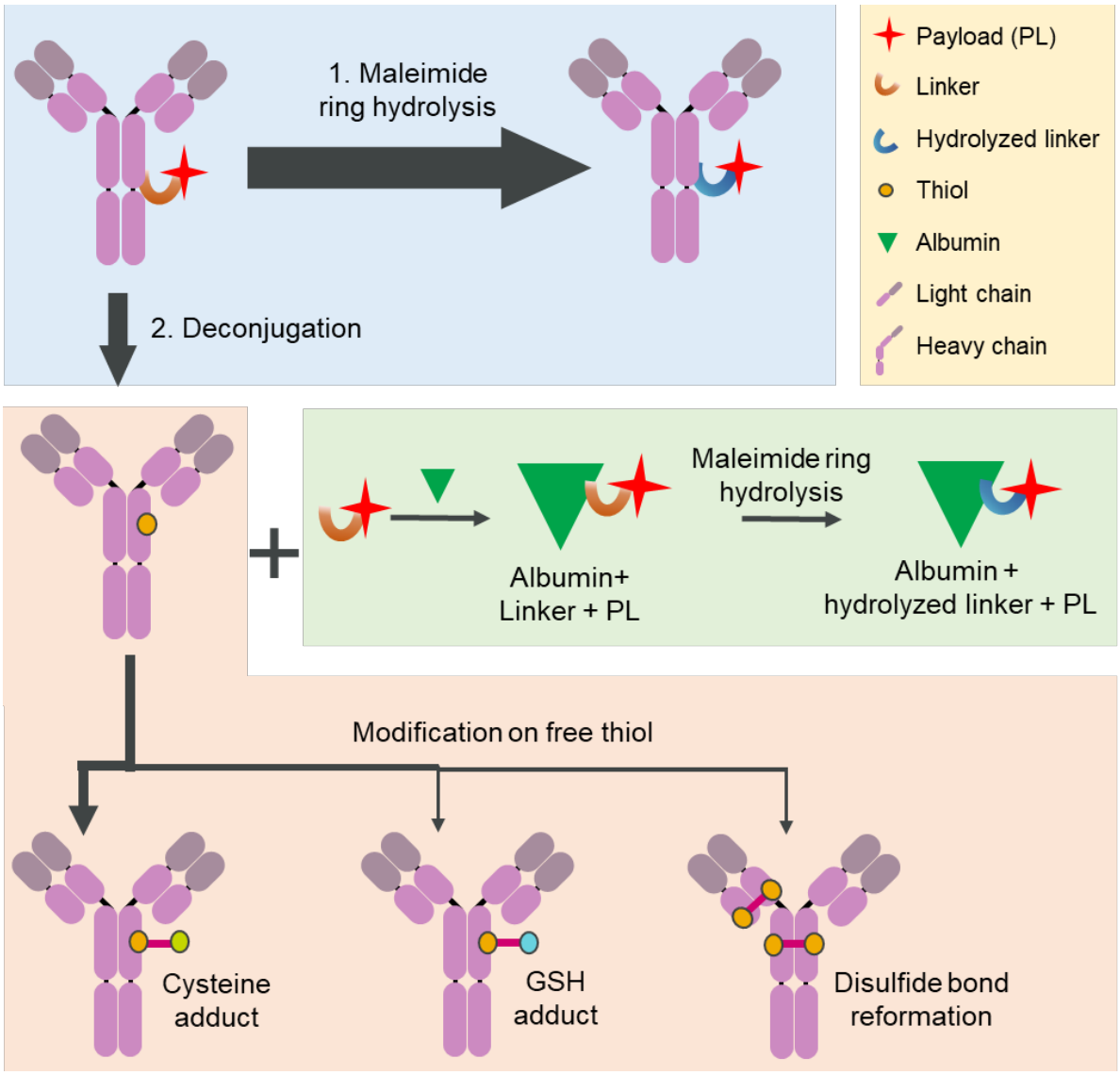

Figure 5. Biotransformation pathway diagram for the ADCs. Blue box highlights the first step of biotransformation pathway, where the linker maleimide ring is either hydrolyzed, stabilizing the conjugation or deconjugated, exposing the free thiol. Following deconjugation the various components of the ADC can then each go through additional biotransformation reactions. Arrow thickness indicates preponderance of biotransformation pathways.

Discussion

Understanding the underlying mechanisms behind the ADC biotransformation is critical to advance the drug candidate through discovery and development[20]. While for small molecule drug candidates, the ADME studies and metabolite ID analysis is routinely performed, the biotransformation of

therapeutic proteins is technically highly challenging. At the meantime, there is an urgent need for understanding the comprehensive biotransformation profile of therapeutic proteins, because of the rapidly increasing diversity of complex therapeutic protein formats, and the resulting knowledge gap in connecting SAR to drug efficacy and safety.

Biotransformation assessments for therapeutic proteins to-date have largely focused on characterizing amino acid post-translational modifications (PTMs) located in critical regions, proteolytic degradation and glycation or glycosylation[21]. For ADCs, linker/payload stability is often the focus of biotransformation characterization[11, 14]. Payload chemical modification such as deacetylation, adduct formation and partial cleavage have been reported. However, the existing gaps in our understanding of ADC SAR make it essential to further elucidate ADC biotransformation profile of the three critical components determining ADC SAR: the protein scaffold, the conjugation site, and the conjugated payload.

For ADCs, SAR depends not only on the binding properties of the CDRs, but also heavily related to the characteristics of the conjugation site and chemistry, linker, and payload[22-24]. The comprehensive profiling of AZD8205 biotransformations demonstrated that the critical structural determinant contributing to the design of this ADC was the PEG section of the linker. The PEG linker resulted in increased maleimide hydrolysis rate (**Figure** 3B). While this resulted also in initial increase in deconjugation rate, after approximately 72 hours post-dose the deconjugation rate was reduced by the competing maleimide hydrolysis reaction allowing AZD8205 to effectively maintain a high DAR ratio throughout the dosing period (**Figure**s 3A and S7B). Thus, quantitative biotransformation profiling across time can be an informative tool to assess the impact of various structural components on the ADC *in vivo* stability.

Building upon our comprehensive characterization of AZD8205 biotransformation we can glean the various biochemical reactions that enable us to obtain more mechanistic understanding of ADC biotransformation pathways. This is particularly important from translational ADME point of view, as such knowledge would be important to understand the translatability of PK and PD data between animal models and the clinical setting. In addition to the known role of proteases in protein degradation, other endogenous molecules and microenvironments may influence ADC biotransformation. One avenue for interrogating the mechanisms of ADC biotransformation is by examining the endogenous molecules covalently and non-covalently associated with ADCs or their catabolites. Redox pairs such as cysteine and GSH have been observed to interact with AZD8205 and its catabolites. Further understanding of the determinants behind these interactions may provide further supporting evidence in translating these preclinical study results to patients.

Understanding drug metabolism is a critical component for successful drug development[3]. Complex macromolecules such as ADCs present unique challenges to gain such understanding. Therefore, we developed and employed several analytical approaches to profile ADC biotransformation in circulation comprehensively. The results help to better understand factors affecting the underlying pharmacokinetic profiles of the various molecular species which are formed when AZD8205 is administered *in vivo*, and thereby aid in developing better understanding of SAR for maleimide-linked ADCs. In the future, these findings could better inform translation of PK/PD from animal models to the clinical setting. Biotransformation profiling of protein conjugates can be further studied in patient populations, or in specific organ/tissue with this or similar method.

Conclusion

In conclusion, we have presented a comprehensive profiling approach focused on the *in vivo* biotransformation pathway for a series of ADCs with differing linkers. We employed immuno-affinity capture enrichment, coupled with reversed phase liquid chromatography and HRMS, to obtain characterization data at a protein subunit level. The data were collected and interpreted with an unbiased deconvolution method. The key biotransformation species can be identified with intact mass and fragmentation, and relative quantification can be performed based on the peak area. The elimination of the parent molecule and generation of the biotransformed species as function of time post-dose can be used to map the biotransformation reaction pathway of the ADC molecules. When applying this methodology in concert, to a group of ADCs, the structure-stability relationship can be established informing the selection of AZ14170133 as optimal linker-payload resulting in AZD8205 ADC. This methodology can be applied to the future development of bioconjugates as potential drug candidates. While the biotransformation in circulation for a group of cysteine-conjugated ADC have been studied extensively here, ADC biotransformation may depend on the linker, the payload or sequences around the conjugation site. In the future, in order to expand our understanding of bioconjugate and catabolites interactions with endogenous molecules, we will need to apply this methodology, across bioconjugates with varying conjugation approaches, linkers and payloads. Notably, it will also be important to evaluate biotransformation pathway in various microenvironments either in specific organs/tissues or tumor to fully understand the determinants for their efficacy/safety profile. Eventually, the biotransformation information obtained in animal models/*in vitro* experiments may be translated to potential patient population as part of clinical studies.

Acknowledgment:
Y.H., H.Y.T., J. Yuan, R.M., J. Yang, K.B., B.V., L.M., K.K., N.L., M.L., and A.I.R. are or were employees of AstraZeneca at the time this work was conducted and may hold stock ownership and/or stock options or interests in the company. This study was funded by AstraZeneca.

References

(1) Petrotchenko, E. V.; Borchers, C. H. Protein Chemistry Combined with Mass Spectrometry for Protein Structure Determination. *Chem Rev* **2022**, *122* (8), 7488-7499. DOI: 10.1021/acs.chemrev.1c00302.
(2) Skinner, O. S.; Haverland, N. A.; Fornelli, L.; Melani, R. D.; Do Vale, L. H. F.; Seckler, H. S.; Doubleday, P. F.; Schachner, L. F.; Srzentic, K.; Kelleher, N. L.; et al. Top-down characterization of endogenous protein complexes with native proteomics. *Nat Chem Biol* **2018**, *14* (1), 36-41. DOI: 10.1038/nchembio.2515.
(3) Schadt, S.; Hauri, S.; Lopes, F.; Edelmann, M. R.; Staack, R. F.; Villasenor, R.; Kettenberger, H.; Roth, A. B.; Schuler, F.; Richter, W. F.; et al. Are Biotransformation Studies of Therapeutic Proteins Needed? Scientific Considerations and Technical Challenges. *Drug Metab Dispos* **2019**, *47* (12), 1443-1456. DOI: 10.1124/dmd.119.088997.
(4) Mu, R.; Yuan, J.; Huang, Y.; Meissen, J. K.; Mou, S.; Liang, M.; Rosenbaum, A. I. Bioanalytical Methods and Strategic Perspectives Addressing the Rising Complexity of Novel Bioconjugates and Delivery Routes for Biotherapeutics. *BioDrugs* **2022**, *36* (2), 181-196. DOI: 10.1007/s40259-022-00518-w.

(5) Hall, M. P. Biotransformation and in vivo stability of protein biotherapeutics: impact on candidate selection and pharmacokinetic profiling. *Drug Metab Dispos* **2014**, *42* (11), 1873-1880. DOI: 10.1124/dmd.114.058347.
(6) Szijj, P. A.; Bahou, C.; Chudasama, V. Minireview: Addressing the retro-Michael instability of maleimide bioconjugates. *Drug Discov Today Technol* **2018**, *30*, 27-34. DOI: 10.1016/j.ddtec.2018.07.002.
(7) Huang, Y.; Mou, S.; Wang, Y.; Mu, R.; Liang, M.; Rosenbaum, A. I. Characterization of Antibody-Drug Conjugate Pharmacokinetics and in Vivo Biotransformation Using Quantitative Intact LC-HRMS and Surrogate Analyte LC-MRM. *Anal Chem* **2021**, *93* (15), 6135-6144. DOI: 10.1021/acs.analchem.0c05376.
(8) Hyung, S. J.; Leipold, D. D.; Lee, D. W.; Kaur, S.; Saad, O. M. Multiplexed Quantitative Analysis of Antibody-Drug Conjugates with Labile CBI-Dimer Payloads In Vivo Using Immunoaffinity LC-MS/MS. *Anal Chem* **2022**, *94* (2), 1158-1168. DOI: 10.1021/acs.analchem.1c04338.
(9) Joubert, N.; Beck, A.; Dumontet, C.; Denevault-Sabourin, C. Antibody-Drug Conjugates: The Last Decade. *Pharmaceuticals (Basel)* **2020**, *13* (9). DOI: 10.3390/ph13090245.
(10) Shen, L.; Sun, X.; Chen, Z.; Guo, Y.; Shen, Z.; Song, Y.; Xin, W.; Ding, H.; Ma, X.; Xu, W.; Zhou, W.; Che, J.; Tan, L.; Chen, L.; Chen, S.; Dong, X.; Fang, L.; Zhu, F. ADCdb: the database of antibody-drug conjugates. *Nucleic Acids Research* **2024**, 52, D1097-D1109
(11) Su, D.; Zhang, D. Linker Design Impacts Antibody-Drug Conjugate Pharmacokinetics and Efficacy via Modulating the Stability and Payload Release Efficiency. *Front Pharmacol* **2021**, *12*, 687926. DOI: 10.3389/fphar.2021.687926.
(12) Shen, B. Q.; Xu, K.; Liu, L.; Raab, H.; Bhakta, S.; Kenrick, M.; Parsons-Reponte, K. L.; Tien, J.; Yu, S. F.; Mai, E.; et al. Conjugation site modulates the in vivo stability and therapeutic activity of antibody-drug conjugates. *Nat Biotechnol* **2012**, *30* (2), 184-189. DOI: 10.1038/nbt.2108.
(13) Zhu, X.; Huo, S.; Xue, C.; An, B.; Qu, J. Current LC-MS-based strategies for characterization and quantification of antibody-drug conjugates. *J Pharm Anal* **2020**, *10* (3), 209-220. DOI: 10.1016/j.jpha.2020.05.008.
(14) He, J.; Yu, S. F.; Yee, S.; Kaur, S.; Xu, K. Characterization of in vivo biotransformations for trastuzumab emtansine by high-resolution accurate-mass mass spectrometry. *MAbs* **2018**, *10* (7), 960-967. DOI: 10.1080/19420862.2018.1494487.
(15) Kotapati, S.; Passmore, D.; Yamazoe, S.; Sanku, R. K. K.; Cong, Q.; Poudel, Y. B.; Chowdari, N. S.; Gangwar, S.; Rao, C.; Rangan, V. S.; et al. Universal Affinity Capture Liquid Chromatography-Mass Spectrometry Assay for Evaluation of Biotransformation of Site-Specific Antibody Drug Conjugates in Preclinical Studies. *Anal Chem* **2020**, *92* (2), 2065-2073. DOI: 10.1021/acs.analchem.9b04572.
(16) Kinneer, K.; Wortmann, P.; Cooper, Z. A.; Dickinson, N. J.; Masterson, L.; Cailleau, T.; Hutchinson, I.; Vijayakrishnan, B.; McFarlane, M.; Ball, K.; et al. Design and Preclinical Evaluation of a Novel B7-H4-Directed Antibody-Drug Conjugate, AZD8205, Alone and in Combination with the PARP1-Selective Inhibitor AZD5305. *Clin Cancer Res* **2022**. DOI: 10.1158/1078-0432.CCR-22-2630 From NLM Publisher.
(17) Kinneer, K.; Dickinson, N. J.; Masterson, L.; Cailleau, T.; Hutchinson, I.; Vijayakrishnan, B.; Dimasi, N.; Christie, R. J.; McFarlane, M.; Ball, K.; et al. Abstract 1765: Discovery and first disclosure of AZD8205, a B7-H4-targeted antibody-drug conjugate utilizing a novel topoisomerase I linker-warhead. *Cancer Research* **2022**, *82* (12_Supplement), 1765-1765. DOI: 10.1158/1538-7445.AM2022-1765 %J Cancer Research (acccessed 10/13/2022).
(18) Meric-Bernstam, F.; Oh, D.-Y.; Naito, Y.; Shimizu, T.; Chung, V.; Park, H.; Gaillard, S.; Wang, F.; Cooper, Z. A.; Kinneer, K.; et al. First-in-human study of the B7-H4 antibody-drug conjugate (ADC) AZD8205 in patients with advanced/metastatic solid tumors. **2022**, *40* (16_suppl), TPS3153-TPS3153. DOI: 10.1200/JCO.2022.40.16_suppl.TPS3153.
(19) Huang, Y.; Del Nagro, C. J.; Balic, K.; Mylott, W. R., Jr.; Ismaiel, O. A.; Ma, E.; Faria, M.; Wheeler, A. M.; Yuan, M.; Waldron, M. P.; et al. Multifaceted Bioanalytical Methods for the Comprehensive Pharmacokinetic and Catabolic Assessment of MEDI3726, an Anti-Prostate-Specific Membrane Antigen

Pyrrolobenzodiazepine Antibody-Drug Conjugate. *Anal Chem* **2020**, *92* (16), 11135-11144. DOI: 10.1021/acs.analchem.0c01187.
(20) Khojasteh, S. C.; Argikar, U. A.; Cho, S.; Crouch, R.; Heck, C. J. S.; Johnson, K. M.; Kalgutkar, A. S.; King, L.; Maw, H. H.; Seneviratne, H. K.; et al. Biotransformation novel advances - 2021 year in review. *Drug Metab Rev* **2022**, *54* (3), 207-245. DOI: 10.1080/03602532.2022.2097253.
(21) Kellie, J. F.; Pannullo, K. E.; Li, Y.; Fraley, K.; Mayer, A.; Sychterz, C. J.; Szapacs, M. E.; Karlinsey, M. Z. Antibody Subunit LC-MS Analysis for Pharmacokinetic and Biotransformation Determination from In-Life Studies for Complex Biotherapeutics. *Anal Chem* **2020**, *92* (12), 8268-8277. DOI: 10.1021/acs.analchem.0c00520.
(22) You, J.; Zhang, J.; Wang, J.; Jin, M. Cysteine-Based Coupling: Challenges and Solutions. *Bioconjug Chem* **2021**, *32* (8), 1525-1534. DOI: 10.1021/acs.bioconjchem.1c00213.
(23) Chowdari, N. S.; Zhang, Y.; McDonald, I.; Johnson, W.; Langley, D. R.; Sivaprakasam, P.; Mate, R.; Huynh, T.; Kotapati, S.; Deshpande, M.; et al. Design, Synthesis, and Structure-Activity Relationships of Novel Tetrahydroisoquinolino Benzodiazepine Dimer Antitumor Agents and Their Application in Antibody-Drug Conjugates. *J Med Chem* **2020**, *63* (22), 13913-13950. DOI: 10.1021/acs.jmedchem.0c01385.
(24) Mantaj, J.; Jackson, P. J.; Rahman, K. M.; Thurston, D. E. From Anthramycin to Pyrrolobenzodiazepine (PBD)-Containing Antibody-Drug Conjugates (ADCs). *Angew Chem Int Ed Engl* **2017**, *56* (2), 462-488. DOI: 10.1002/anie.201510610.

Supporting Information

Extensive Biotransformation Profiling of AZD8205, an Anti-B7-H4 Antibody-Drug Conjugate, Elucidates Pathways Underlying its Stability In Vivo

Yue Huang[1], Hui Yin Tan[1], Jiaqi Yuan[1], Ruipeng Mu[1], Junyan Yang[1], Kathryn Ball[2], Balakumar Vijayakrishnan[3], Krista Kinneer[4], Nadia Luheshi[5], Meina Liang[1], Anton I. Rosenbaum[1]

[1]*Integrated Bioanalysis, Clinical Pharmacology and Safety Sciences, R&D, AstraZeneca, South San Francisco, CA 94080, USA*

[2]*Clinical Pharmacology and Quantitative Pharmacology, Clinical Pharmacology and Safety Sciences, R&D, AstraZeneca, Cambridge CB21 6GH United Kingdom*

[3]*TTD, Oncology R&D, AstraZeneca, London E1 2AX, United Kingdom*

[4]*Translational Medicine, Oncology, AstraZeneca, Gaithersburg, MD 20878, USA*

[5] *Oncology R&D, Cambridge CB2 8PA, United Kingdom*

***Corresponding Authors**

Yue Huang - *121 Oyster Point Blvd, South San Francisco, CA 94080, USA*; Tel: +1-650-481-6801 ;E-mail: yhuang@revmed.com

Anton I. Rosenbaum - *121 Oyster Point Blvd, South San Francisco, CA 94080, USA*; Tel: +1-650-379-3099; E-mail: anton.rosenbaum@astrazeneca.com

Index No.	ADC	dose (mg/kg)	time point (h)	ADC Conc (µg/mL)	Volume for 1 µg (µL)	Pooled Plasma Volume (µL)	Actual Volume (µL)	Actual Amount (µg)
1	ADC1	5	0.5	100.04	10.0	110.0		1
2		5	6	55.68	18.0	102.0		1
3		5	24	32.22	31.0	89.0		1
4		5	48	19.87	50.3	69.7		1
5		5	144	8.31	120.4	NA	120.4	1
6		5	288	3.29	303.6	NA	200	0.66
7	ADC2	5	0.5	115.39	8.7	111.3		1
8		5	6	45.44	22.0	98.0		1
9		5	24	25.46	39.3	80.7		1
10		5	48	20.28	49.3	70.7		1
11		5	144	8.65	115.6	4.4		1
12		5	288	3.51	285.2	NA	200	0.70
13	ADC4	5	0.5	112.63	8.9	111.1		1
14		5	6	54.07	18.5	101.5		1
15		5	24	21.14	47.3	72.7		1
16		5	48	18.64	53.7	66.3		1
17		5	144	2.34	428.2	NA	130	0.30
18		5	288	1.81	552.9	NA	150	0.27
19	ADC3	5	0.5	107.48	9.3	110.7		1
20		5	6	45.55	22.0	98.0		1
21		5	24	24.03	41.6	78.4		1
22		5	48	19.06	52.5	67.5		1
23		5	144	8.70	114.9	5.1		1
24		5	288	2.35	425.2	NA	200	0.47

Table S1: Mouse plasma sample information for intact LC-HRMS biotransformation experiment design. The known plasma concentration from the LC-MRM assay was used to calculate the volume needed for 1 ug of ADC extraction.

ADC	Detection	AUC_{last} day*ug/mL	C_{max} ug/mL	CL mL/day/kg	$T_{1/2, z}$ day	V_{ss} mL/kg
ADC1 B7H4-AZ14170133	Conj ADC	136	93.0	34.1	3.48	143
	HC	141	94.7	32.9	3.48	139
	LC	130	98.8	36.5	2.95	135
ADC2 B7H4-AZ14208669	Conj ADC	141	105	31.4	3.77	153
	HC	144	95.8	30.1	4.11	163
	LC	144	98.7	30.9	3.68	148
ADC3 B7H4-AZ14208672	Conj ADC	132	102	35.9	2.97	131
	HC	137	102	34.3	3.13	134
	LC	135	92.8	34.5	3.14	146
ADC4 B7H4-AZ14208670	Conj ADC	123	104	39.1	2.56	117
	HC	128	107	37.5	2.61	116
	LC	134	105	35.7	2.66	115

Table S2: Pharmacokinetic parameters of ADC1-4 in Tg32 mice. AUC: area under the plasma concentration–time curve. Cmax: maximum serum concentration. CL: plasma clearance. Vss: volume of distribution at steady state (Vss). T1/2, z: terminal elimination half-life. Conj: Conjugated.

Component (Species) Name	Mass extraction range (Da)
Cytochrome C	12361.3400 - 12362.5800
LC + 1Payload	24642.4600 - 24644.9200
LC + 1Payload + 1H2O	24660.4600 - 24662.9200
LC	23494.2500 - 23496.5900
HC + G0F	50296.7800 - 50301.8000
HC + G1F	50458.7700 - 50463.8100
HC + 1Payload + G0F	51444.9900 - 51450.1300
HC + 1Payload + G1F	51606.9800 - 51612.1400
HC + 1Payload + G0F + 1H2O	51462.9900 - 51468.1300
HC + 1Payload + G1F + 1H2O	51624.9800 - 51630.1400
HC + 2Payload + G0F	52593.2000 - 52598.4600
HC + 2Payload + G1F	52755.1900 - 52760.4700
HC + 2Payload + G0F + 1H2O	52611.2000 - 52616.4600
HC + 2Payload + G1F + 1H2O	52773.1900 - 52778.4700
HC + 2Payload + G0F + 2H2O	52629.2000 - 52634.4600
HC + 2Payload + G1F + 2H2O	52791.1900 - 52796.4700
HC + 2Payload + G0F + Cys	52713.1900 - 52718.4700
HC + 2Payload + G1F + Cys	52875.1900 - 52880.4700
HC + 2Payload + G0F + 1H2O + Cys	52731.1900 - 52736.4700
HC + 2Payload + G1F + 1H2O + Cys	52893.1900 - 52898.4700
HC + 2Payload + G0F + 2H2O + Cys	52749.1900 - 52754.4700
HC + 2Payload + G1F + 2H2O + Cys	52911.1800 - 52916.4800
HC + 3Payload + G0F	53741.4100 - 53746.7900
HC + 3Payload + G1F	53903.4000 - 53908.8000
HC + 3Payload + G0F + 1H2O	53759.4100 - 53764.7900
HC + 3Payload + G1F + 1H2O	53921.4000 - 53926.8000
HC + 3Payload + G0F + 2H2O	53777.4100 - 53782.7900
HC + 3Payload + G1F + 2H2O	53939.4000 - 53944.8000
HC + 3Payload + G0F + 3H2O	53795.4100 - 53800.7900
HC + 3Payload + G1F + 3H2O	53957.4000 - 53962.8000
LC + HC + 2Payload + G0F	76087.4500 - 76095.0500
LC + HC + 2Payload + G1F	76249.4400 - 76257.0600
LC + HC + 2Payload + G0F + 1H2O	76105.4400 - 76113.0600
LC + HC + 2Payload + G1F + 1H2O	76267.4400 - 76275.0600
LC + HC + 2Payload + G0F + 2H2O	76123.4400 - 76131.0600
LC + HC + 2Payload + G1F + 2H2O	76285.4400 - 76293.0600
LC + Cys	23614.2400 - 23616.6000
HC + 1Payload + G0F +1Cys	51564.9800 - 51570.1400
HC + 1Payload + G1F +1Cys	51726.9700 - 51732.1500
HC + 1Payload + G0F + 1H2O +1Cys	51582.9800 - 51588.1400
HC + 1Payload + G1F + 1H2O +1Cys	51744.9700 - 51750.1500
HC + 1Payload + G0F +2Cys	51684.9800 - 51690.1400
HC + 1Payload + G1F +2Cys	51846.9700 - 51852.1500
HC + 1Payload + G0F + 1H2O +2Cys	51702.9700 - 51708.1500
HC + 1Payload + G1F + 1H2O +2Cys	51864.9700 - 51870.1500

Table S3: MultiQuant extraction mass range example (ADC 1, AZD8205) for deconvoluted mass-time chromatogram generated from PeakView (research version).

Biotransformation	Key Section of the Biotransformation Species	Theoretical m/z	z
LC hydrolysis	GEC+1hydrolyzed linker + 1PL	491.8834	3
HC hydrolysis (Fig S3)	SCDK+1hydrolyzed linker + 1PL	539.9134	3
HC hydrolysis	THT+2*(hydrolyzed linker + PL))	1013.1065	5
HC Cys (Fig S4)	THT+1*(hydrolyzed linker + PL) + 1Cys	803.7987	5
HC GSH	THT+1*(hydrolyzed linker + PL) + 1GSH	841.0115	5
HC intra SS (Fig S5)	THT intra S-S	682.8558	4
LC+HC inter SS (Fig S6)	GEC+SCDKTHT+2*(hydrolyzed linker + PL)	967.4619	6

Table S4: Confirmed key fragments from enzymatic digestions of selected biotransformation species using the bottom up LBA-LC-HRMS method.

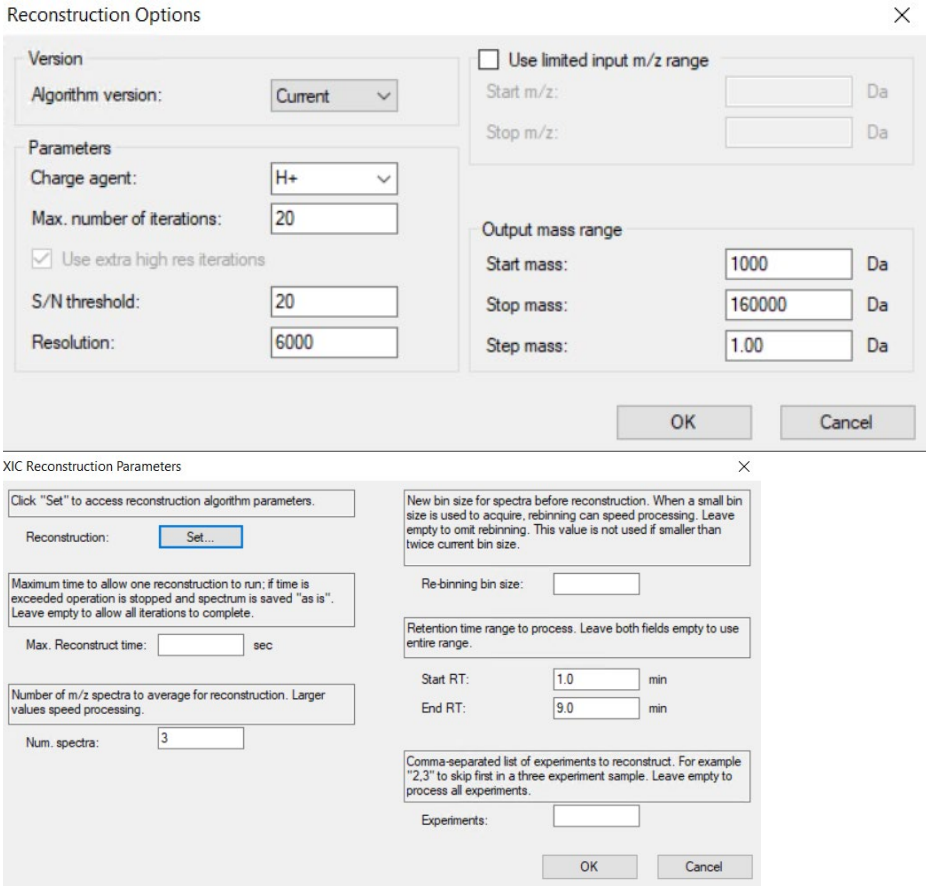

Figure S1: Deconvolution parameters in research version PeakView. The LC-HRMS data is converted from m/z to the mass domain, while maintaining the chromatographic information.

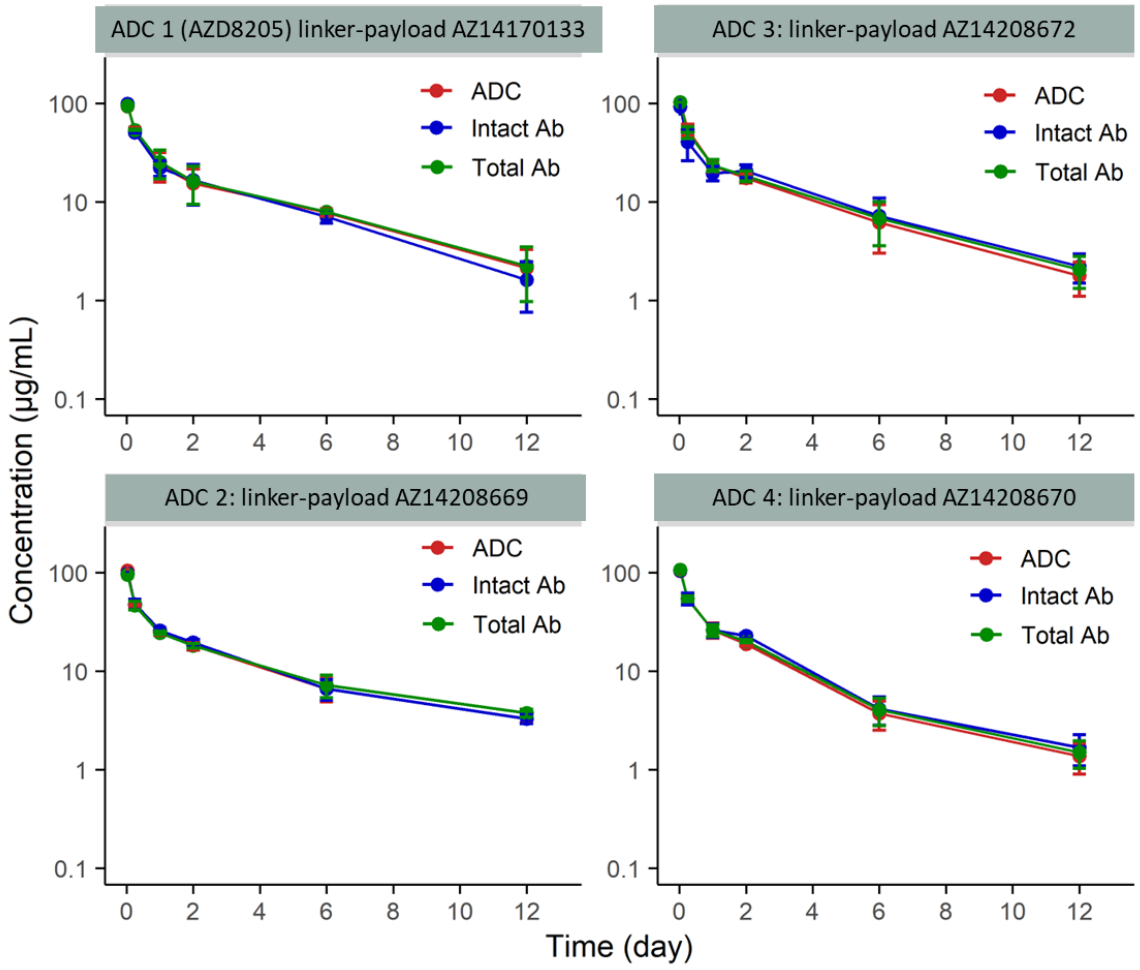

Figure S2. Concentration-time profiles of ADC1-4 after a single bolus 5 mg/kg IV dose in Tg32 mice analyzed by LBA-LC-MRM. The ADC assay captures with the anti-human Fc antibody and detects the payload. The ADC concentration here included both the hydrolyzed and non-hydrolyzed linker.

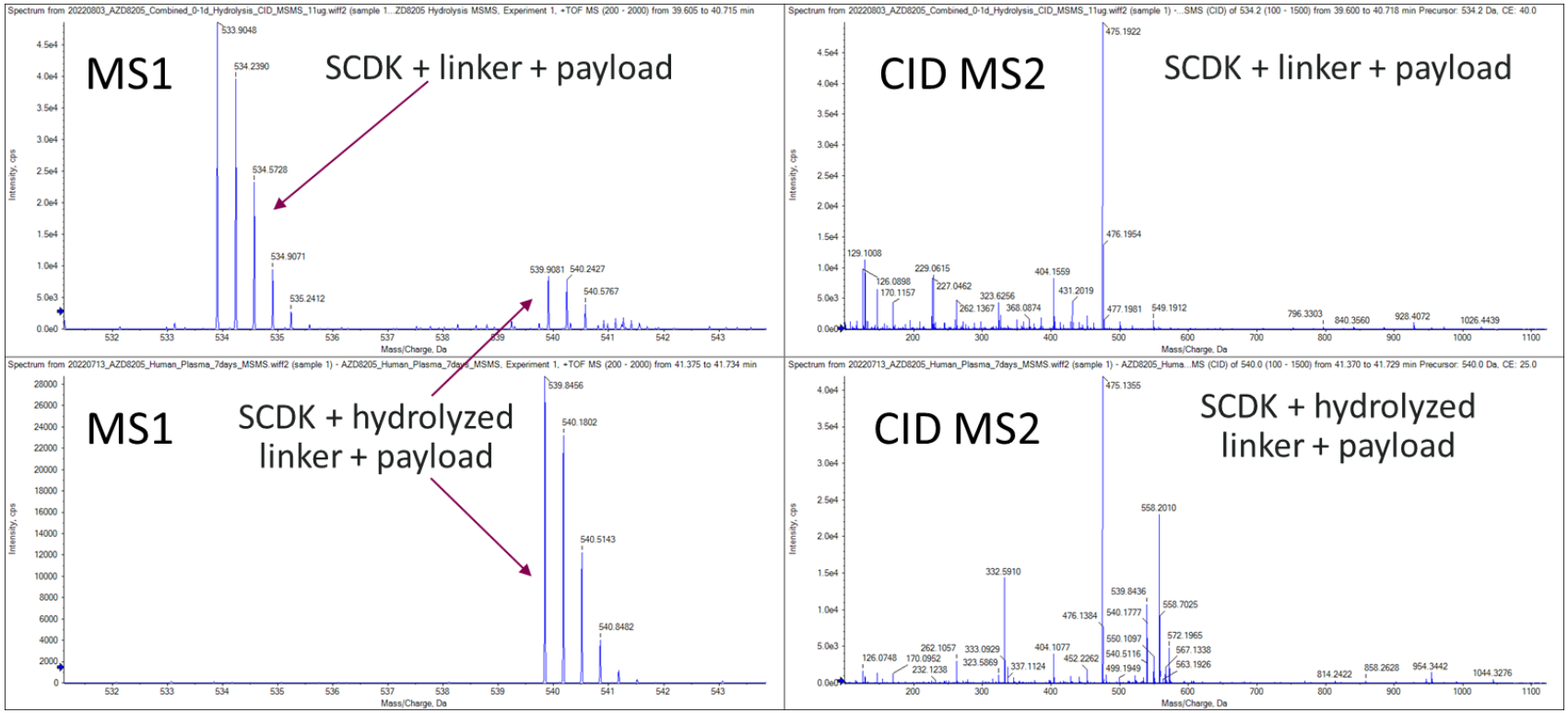

Figure S3. Selected maleimide hydrolysis species confirmed with bottom-up LBA-LC-HRMS. Peptide SCDK is on the heavy chain peptide with linker and payload, conjugated to the C. The spectra are from in vitro plasma incubation samples with 0day incubation (top panels) and 7 days incubation (bottom panels) at 37 °C. The left panels are the MS1 spectra, where the observed mass matched the theoretical mass in table S2. The right panels are the CID fragmentation for the non-hydrolyzed and the hydrolyzed. While a signature fragment from the payload section (475) was observed in both spectra, there is a series of +18 fragment ions indicating the hydrolysis of the sample.

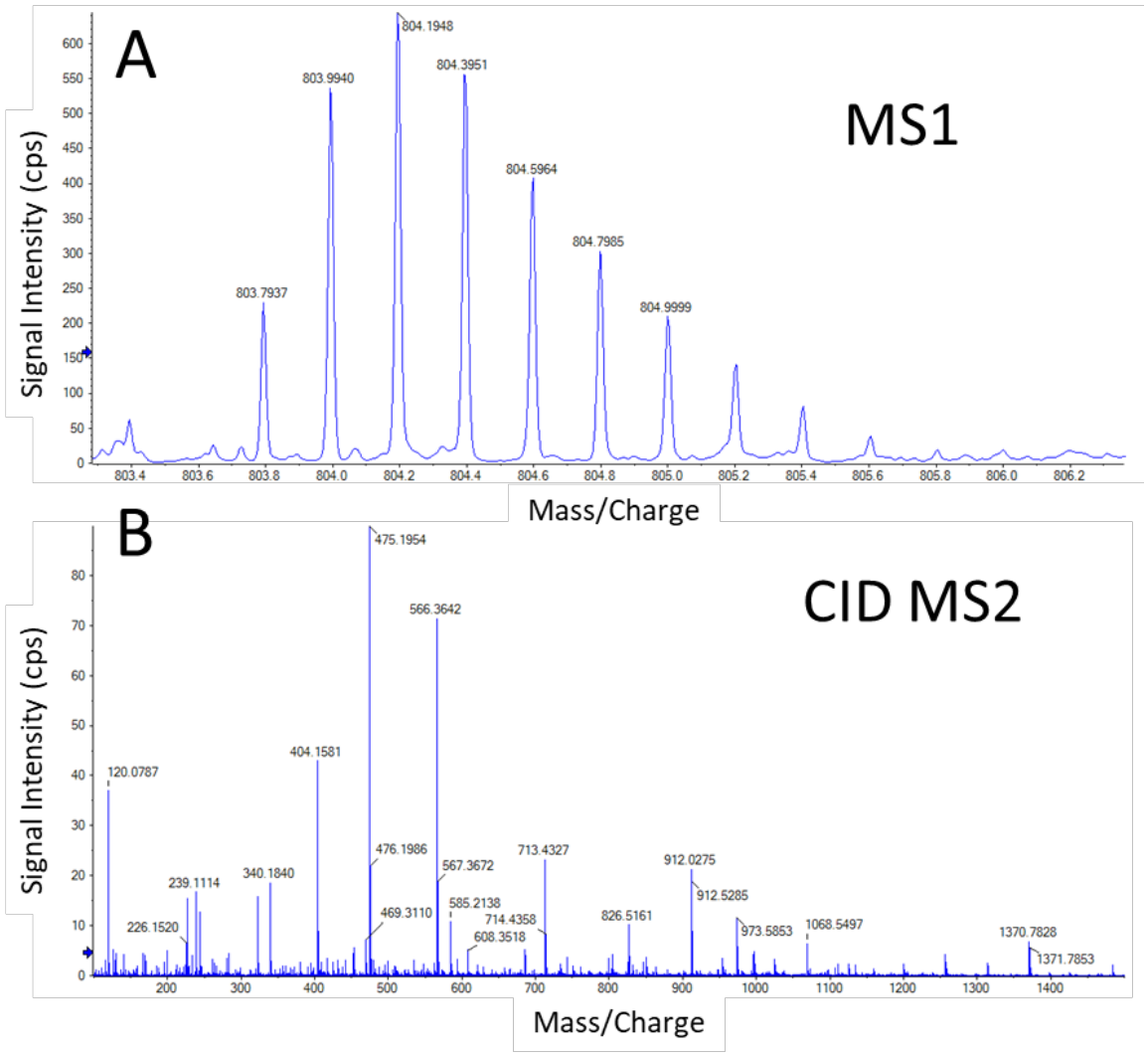

Figure S4. Cysteine adducts confirmed with bottom-up LBA-LC-HRMS. The spectra are from in vitro plasma incubation samples, 7 days at 37 °C. A) MS1 spectra for THTCPPCPAPELLGGPSVFLFPPKPK, the hinge region heavy chain peptide, with one cysteine connected to the hydrolyzed linker and payload and the other cysteine connected to a cysteine. B) MS2 spectra with the signature ion 475 and 404 from the payload, and peptide fragment series for the peptide backbone.

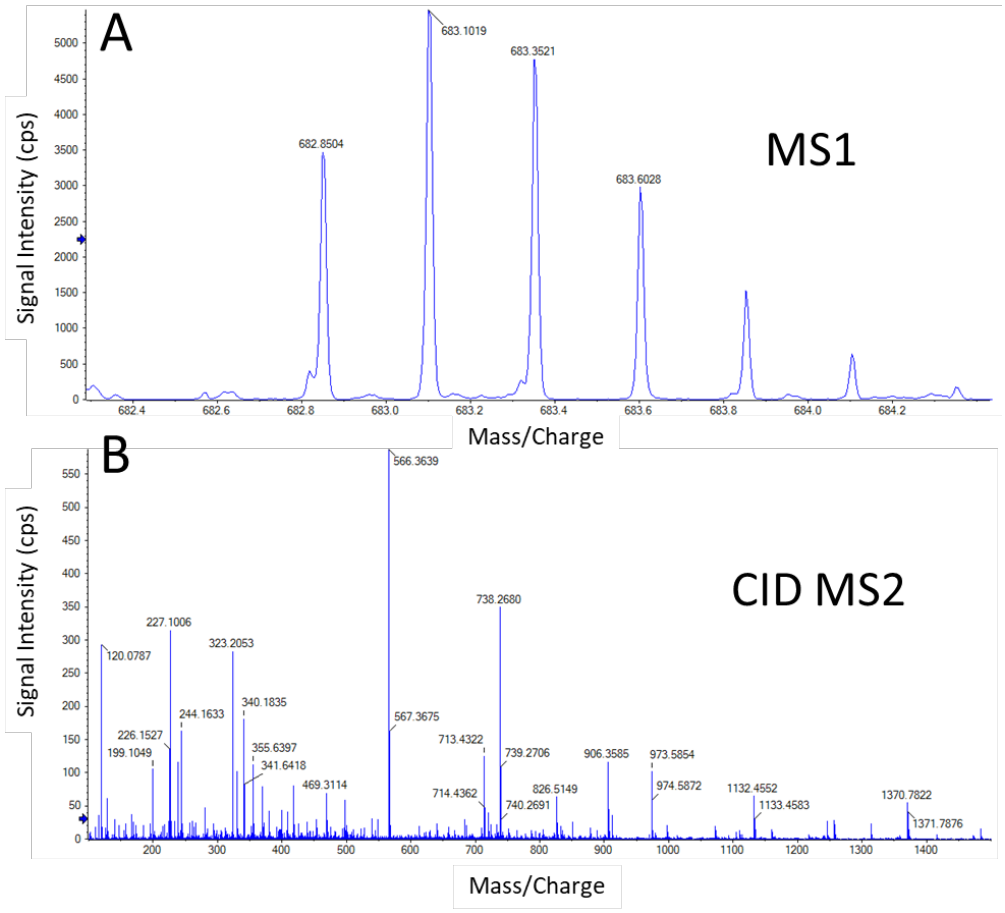

Figure S5. Reformation of intra-chain disulfide bonds confirmed with bottom-up LBA-LC-HRMS. The spectra are from in vitro plasma incubation samples, 7 days at 37 °C. A) MS1 spectra for THTCPPCPAPELLGGPSVFLFPPKPK, the hinge region heavy chain peptide, with the two cysteines forming an intra-chain disulfide bond. B) MS2 spectra with the peptide fragment series for the peptide backbone.

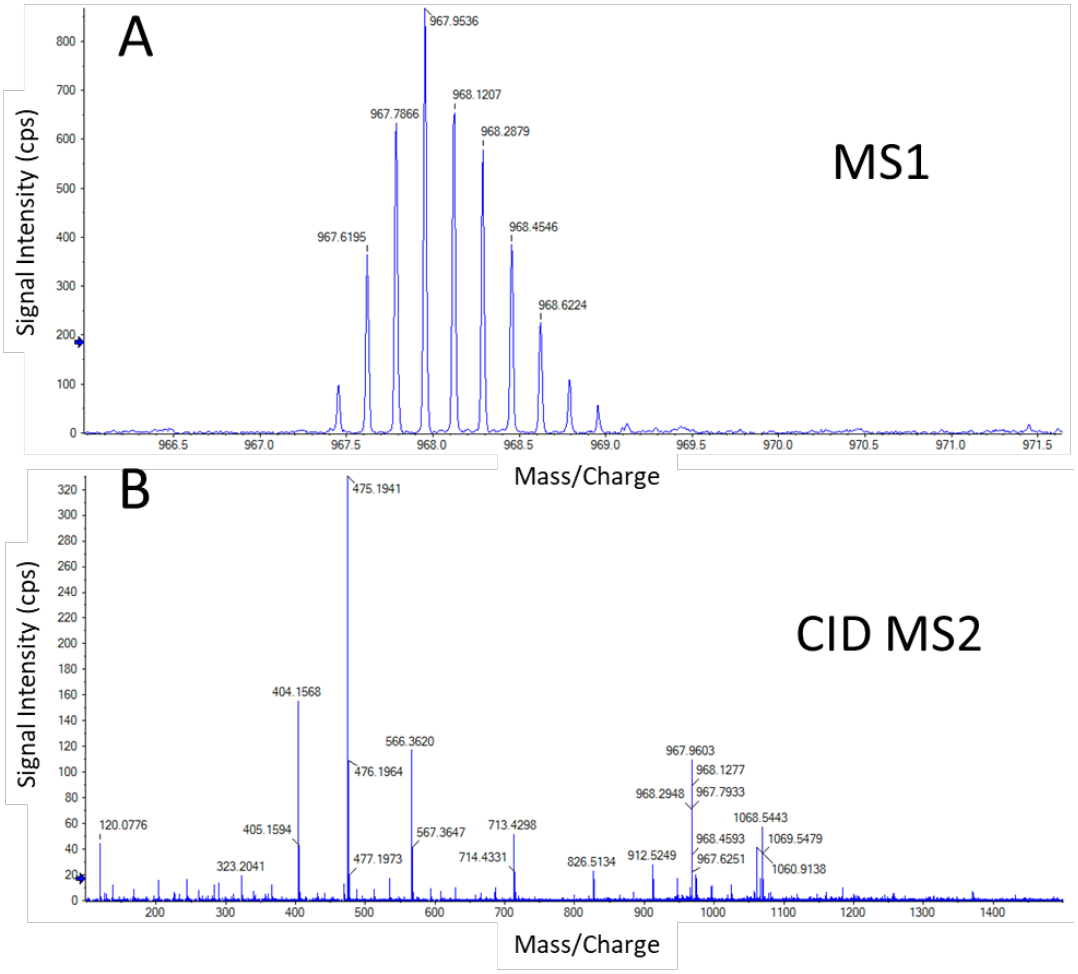

Figure S6. Reformation of inter-chain disulfide bonds confirmed with bottom up LBA-LC-HRMS. The spectra are from in vitro plasma incubation samples, 7 days at 37 °C. A) MS1 spectra for GE***C***__S***C***DKTHTCPPCPAPELLGGPSVFLFPPKPK, the hinge region peptides, with the two cysteines from light chain (GE***C***) and heavy chain (S***C***DK) forming an inter-chain disulfide bond, and two other cysteines (CPPC) connected to hydrolyzed linker with payload B) MS2 spectra with the peptide fragment series for the peptide backbones and the signature ions 475 and 404 from the payload

.

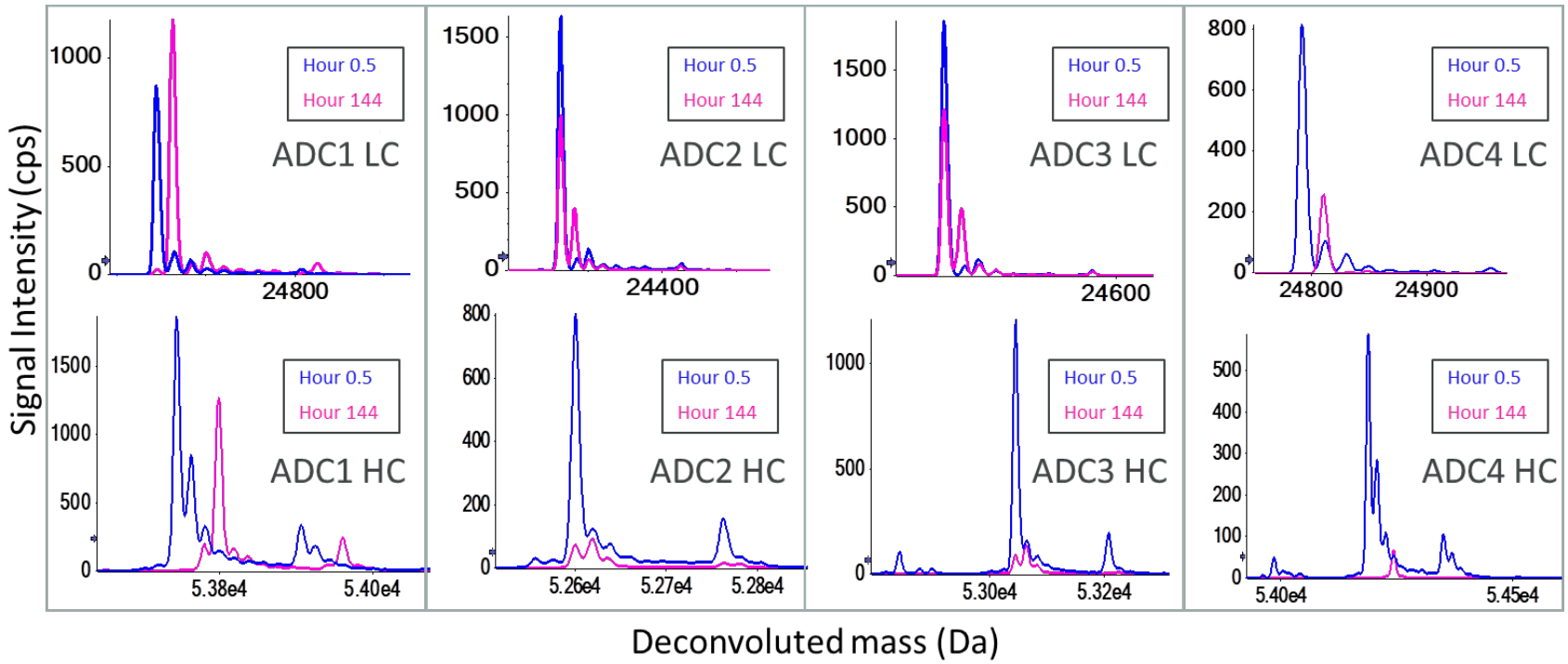

Figure S7. Maleimide hydrolysis at two time points post-dose for the light chain (top) and heavy chain (bottom) for ADCs 1-4, shown with deconvoluted spectra at the time of elution.

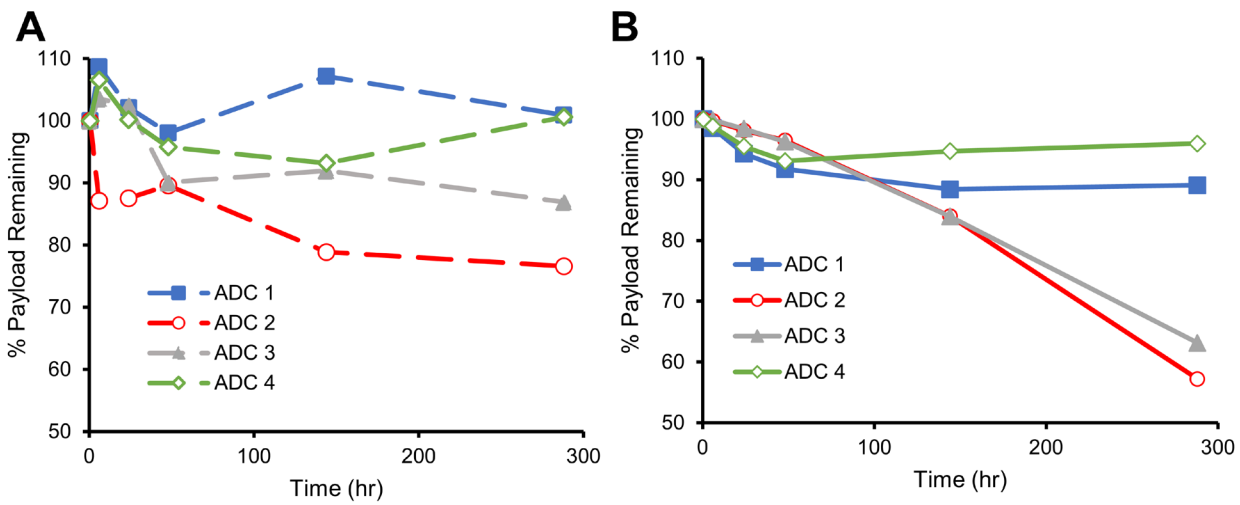

Figure S8. Relative quantification for DAR with LC-MRM method (A) and intact LC-HRMS method (B) for ADC1-4.

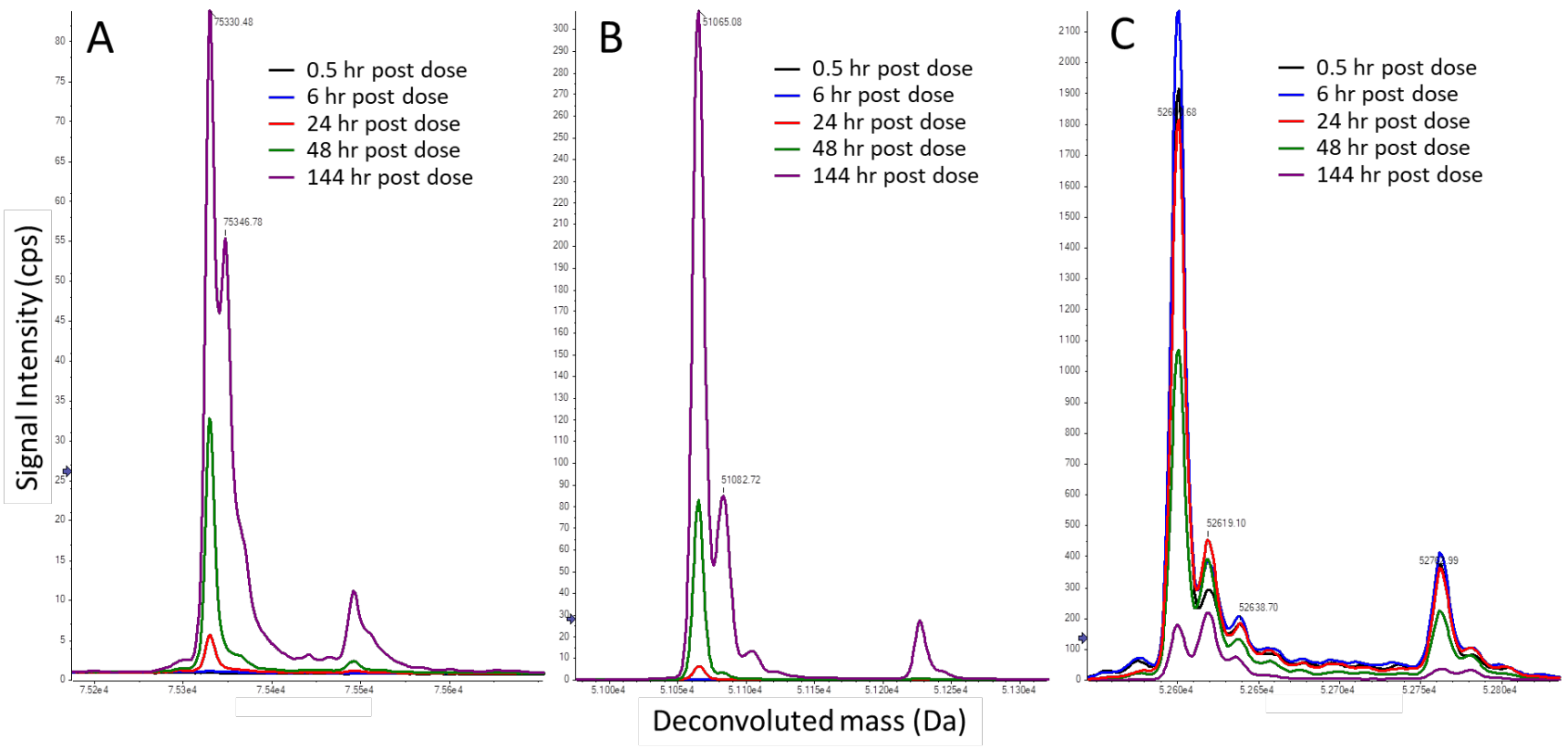

Figure S9. Deconvoluted mass spectra, zoomed in for A) LC-HC reformation, B) heavy chain species with only 1 payload and C) heavy chain species with 2 remaining payloads.

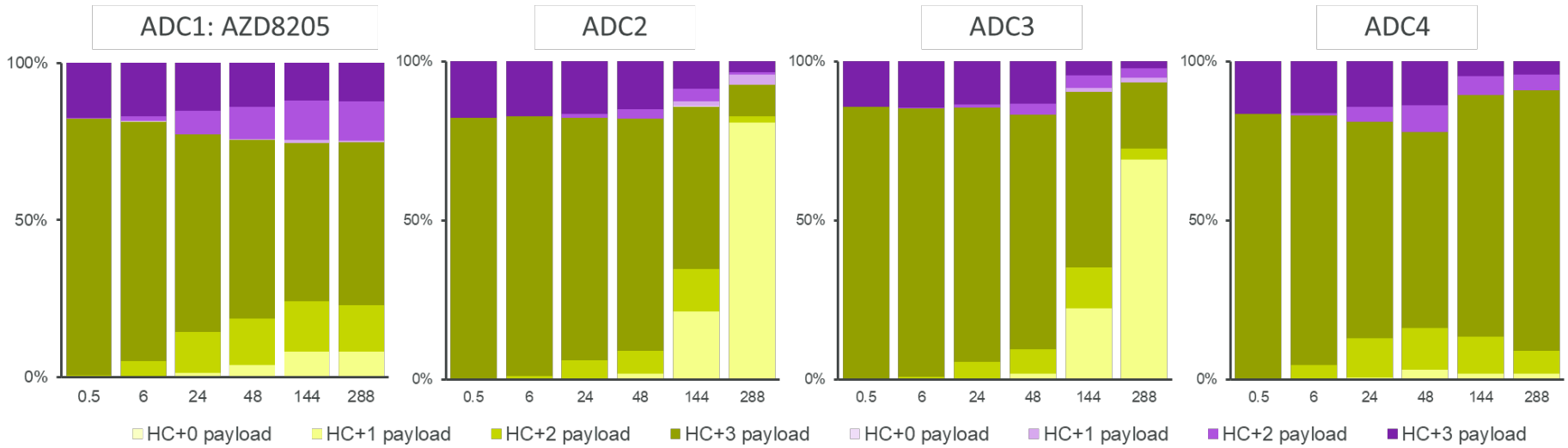

Figure S10. Glycosylation profile of ADCs 1-4. The yellow color is all the G0F species, the purple represented the G1F species. No significant change observed for the glycosylation profiles over the time.